Received: 23 August 2020 | Revised: 9 November 2020 | Accepted: 13 December 2020

DOI: 10.1002/pen.25622

RESEARCH ARTICLE

POLYMER ENGINEERING AND SCIENCE WILEY

Enhanced mandrel design for electrospinning aligned fiber mats from low volatility solvents

Somdatta Bhattacharya[1] | **Corey Woodcock**[1] | **Robert J. Linhardt**[1,2] | **Joel L. Plawsky**[1]

[1]Howard P. Isermann Department of Chemical and Biological Engineering and Center for Biotechnology and Interdisciplinary Studies, Rensselaer Polytechnic Institute, Troy, New York, USA

[2]Department of Chemistry and Chemical Biology, Rensselaer Polytechnic Institute, Troy, New York, USA

Correspondence
Joel L. Plawsky, Howard P. Isermann Department of Chemical and Biological Engineering and Center for Biotechnology and Interdisciplinary Studies, Rensselaer Polytechnic Institute, Troy, NY 12180, USA.
Email: plawsky@rpi.edu

Funding information
Rensselaer Polytechnic Institute; NASA, Grant/Award Number: 80NSSC18K0332

Abstract

A cylindrical mandrel with axially aligned rods was designed and tested for the collection of electrospun fibers. Blended polyaniline/polyethylene oxide fibers were electrospun from a solution containing a nonvolatile solvent, *m*-cresol. Camphorsulfonic acid served as the primary dopant and *m*-cresol were used as the secondary dopant to enhance fiber conductivity. A smooth, rotating cylindrical mandrel collector failed to collect and align fibers and instead afforded a wet, sticky film. An eight-rod, rotating cylindrical mandrel resulted in a dry, aligned fiber mat composed of 7–10 μm diameter fibers. Alignment was maintained for at least 18 h of continuous spinning and the resulting mat could be easily recovered from the mandrel. A simulation of the rotating system indicated that the efficient formation of dry, nonsticky, aligned fiber mat was facilitated by the high mass transfer coefficient associated with the use of corrugated rods. Experiments indicated that 6–10 rods were optimal avoiding sagging of the fibers at the low end and increased mas transfer resistance at the high end.

KEYWORDS

aligned fibers, electrospinning, mandrel design, mass transfer coefficient, nonvolatile solvent

1 | INTRODUCTION

First explored in the 1930s,[1] electrospinning has become a simple and versatile method to produce micrometer or nanometer scale fibers from polymer solutions. Electrospun fibers have large surface area-to-volume ratios, making them very efficient substrates for use in a variety of applications such as the adsorption of chemicals,[2] charge storage,[3,4] drug delivery,[5,6] virus filtration,[7] and tissue engineering.[8,9] The growing interest in producing nanostructured materials has stimulated renewed efforts to enhance electrospinning operations. In a conventional electrospinning configuration, a polymer solution is injected through a hollow needle attached to a spinneret. Upon the application of a high (10–30 kV) voltage to the needle, the polymer droplet at the exit of the needle forms a Taylor cone and encounters sufficient electrostatic force to overcome the surface tension of the polymer solution and eject a very thin stream of polymer from the tip of the cone. This charged jet of polymer undergoes a bending instability, which causes it to rapidly whip in multiple expanding loops as it approaches a grounded, collector surface. This whipping process causes a further stretching and thinning of the fiber until it enters the micrometer and nanometer range. Normally, the stretching and thinning of the fiber promotes solvent evaporation, increasing the solidity and integrity of the polymer fibers.[10]

Electrospinning generally forms nonwoven mats whose morphology has been difficult to control. Recent

studies have investigated different electrospinning approaches by building a variety of complex collector designs aimed at providing control in cospinning/blending, fiber orientation, and targeted collection.[11,12] However, most of these studies have been limited by requiring the use of solvents with significant vapor pressures.[13,14] High volatility solvents are desirable since they efficiently vaporize, allowing the electrospun polymer to form solid fibers before they are collected. The rapid formation of solid fibers enhances the efficiency of electrospinning and results in a nonwoven mat composed of discrete electropun fibers. When low volatility solvents are used in electrospinning, residual solvent remains in the fibers upon collection, making the fiber mat difficult to recover from the collector and often yielding a fused film.[15,16] The challenges faced when electrospinning fibers from low volatility, high boiling point, solvents have not been well addressed and no systematic investigation, of the impact of mass transfer and mandrel design on fiber formation, has been undertaken.

Another challenge of electrospinning fibers is maintaining fiber alignment within a mat. The whipping instability of the Taylor cone makes the collection of aligned fibers challenging. Aligned electrospun fibers are important in producing structures that exhibit unique optical, electrical, and mechanical properties.[17-19] Alignment is most commonly achieved using a rotating mandrel. Most of the techniques used to produce aligned fibers have difficulty retaining fiber alignment for extended periods (i.e., >45 min) of deposition.[17] Thus, most studies report a loss in fiber alignment in thicker mats though there is no standard for reporting alignment over time.[20]

Here, we report a new mandrel design that addresses the challenges of low volatility solvents and fiber alignment. Finite element simulation was used to understand the mass transfer surrounding a newly designed mandrel to and answer the question of whether improved mass transfer at the mandrel surface might be one reason behind the enhanced ability to form aligned fiber mats using low volatility solvents.

2 | MATERIALS AND METHODS

2.1 | Chemicals

Polyaniline (PANI, emeraldine base, average molecular weight of 65,000), poly(ethylene oxide) (PEO, average molecular weight of 2,000,000), (+)-camphor-10-sulfonic acid (CSA), *m*-cresol, and chloroform (high performance liquid chromatography grade) were all purchased from the Sigma-Aldrich, St. Louis, MO. All materials were used without further purification.

2.2 | Sample preparation

A 10 ml mixture of chloroform and *m*-cresol, at volume ratios of 9:1 and 4:1, and CSA (0.087 g) were continuously stirred for 4 h to obtain a uniform solution. PANI (0.068 g) was slowly added to this solution and the mixture was continuously stirred at 25°C for 24 h. The resulting solution was filtered using a 0.45 μm Nylon filter (25 mm in diameter). Finally, PEO (0.085 g) was added and stirred overnight to obtain the final solution for electrospinning.

2.3 | Electrospinning

The potential difference for electrospinning was generated using a high voltage power supply (ES 50P-5 W, Gamma High Voltage Research Inc.). The applied voltage was maintained between 20 and 50 kV in all cases. A monoaxial spinneret (MECC, Ogori, Fukuoka, Japan) with a blunt tip, aluminum needle (23 gauge) having an internal diameter of 0.635 mm was used. The needle tip to collector surface distance was varied between 20 and 23 cm. The flow rate of the solution was controlled using a syringe pump (NE-1000, New Era Pump System Inc., Wantagh, NY) and varied from 1 to 1.5 ml/h. The temperature and the humidity were monitored using a digital humidity and temperature monitor (AcuRite®) and were maintained at 20 ± 3°C and 16%, respectively.

2.4 | Characterization

Fiber morphology was investigated using a Carl Zeiss Supra field emission scanning electron microscope (SEM) (Hillsboro—resolution at 1 kV—2.5 nm). NIH ImageJ software (National Institute of Health, MD) was used to calculate the average fiber diameters. Diameters of approximately 3000 individual fibers from 10 identical electrospinning experiments were employed in our fiber diameter analysis.

2.5 | Modeling and simulation of the mandrel design

Once the polymer jet emerges from the Taylor cone, it is subject to multiple physical forces that define its trajectory toward the collection mandrel. These trajectories or distance traveled, help determine the amount of residual solvent remaining in the polymer once the fiber reaches the collection mandrel and how much solvent still needs to evaporate as the fiber winds onto the surface of the

mandrel. A key component of the mandrel design discussed below is the use of thin (∅6.5 mm), conducting rods aligned axially along the mandrel cylinder. The rods were grounded, providing focal points for fiber collection. We hypothesized that a key element in mandrel design, the use of rods, should favor solvent evaporation and allow the fibers to dry after they were deposited on the mandrel. Thus, the mass transfer coefficient for our mandrel design should be significantly larger than the mass transfer coefficient for a solid cylindrical mandrel if enhanced mass transfer could help explain the improved performance of the design. We developed a simple, finite element model of the mandrel geometry to initially test this hypothesis.

A simplified geometry describes the mandrel design as shown in Figure 1. This design consists of a 10 cm diameter metallic cylinder surrounded by between 6 and 10 equally spaced, 0.25 inch rods. The rods were located 3 mm from the solid mandrel surface and the overall geometry approximated a cross-section from the center of the experimental apparatus. A circular region cutting through the center of the rods was defined as the average location of the fiber mat for the purpose of evaluating the mass transfer coefficient. This accounted for a small amount of fiber sag between the rods. Experimentally, six rods were required to keep the fibers from sagging and touching the solid mandrel surface.

The model incorporated the Navier–Stokes equations for laminar flow about the cylinder coupled with the convective-diffusion equation to understand how quickly the solvent dissipates from the mat surface to the surrounding air. We used no-slip boundary conditions on all the solid surfaces and impermeable conditions on all the external walls, the mandrel surface, and the rods. For the smooth mandrel having no rods, the mandrel surface condition was a constant concentration set at a nominal value of 100 mol/m^3. Thus, this represents the case a short time after the fibers are deposited yet while they are still saturated with *m*-cresol. In the rod mandrel design, the mandrel surface was impermeable and the circle cutting through the rods was held at the same constant concentration of 100 mol/m^3. Simulations were run at room temperature and atmospheric pressure, which defined the physical properties of the air surrounding the mandrel. The point located near the upper right corner of the figure is a pressure constraint point necessary to ensure the simulation would proceed. Equation (1) was used to calculate the mass transfer coefficient and compare the values between smooth and rod-mandrel design.

$$Kc = \frac{N}{A\Delta C}, \tag{1}$$

Kc is the mass transfer coefficient (mol/[s m^2]/[mol/m^3]), or m/s, N is the mass flux (mol/m^{2}s), A is the effective mass transfer area (m^2), and ΔC is the driving force concentration difference (mol/m^3) between the mandrel surface and a point far above the spinneret.

Over the time period of the simulation, long enough to reach a steady-state mass transfer coefficient, the free stream value of the *m*-cresol concentration was assumed to be 0. Since the mandrel was relatively small and the space in which the experiment took place was large, this is not a bad assumption. The mass transfer calculation was started only after the velocity field had reached a steady-state. This mimicked the experimental procedure of starting the mandrel first, getting it up to speed, and then starting the electrospinning process.

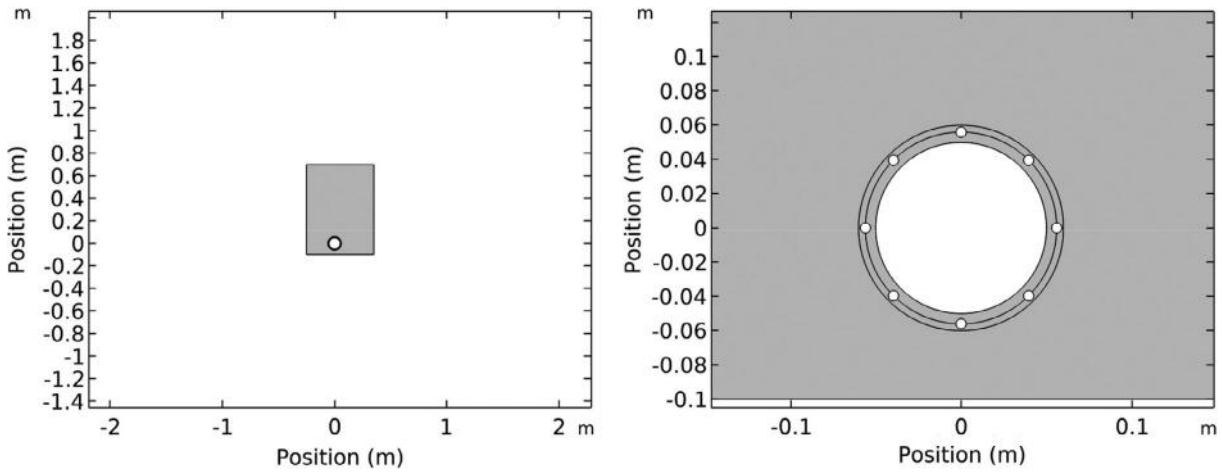

FIGURE 1 Geometry of the mandrel design used in the COMSOL simulation. This mandrel is shown with eight-rods aligned axially along the cylinder

3 | RESULTS AND DISCUSSION

3.1 | Experimental results

Using a smooth mandrel design, the evaporation of the m-cresol solvent from the deposited PANI-PEO fibers was slow. Thus, the PANI-PEO formed a solid sheet, which was hard to remove from the collector surface (Figure 2). SEM clearly showed a sheet-like structure with no individual fibers evident (Figure 2(C,D)).

Eight quarter-inch, threaded rods were prepared and attached to the mandrel surface using two custom collars formed via additive manufacturing (Figure 3). This design provided sufficient airflow between the rods and mandrel surface aiding in the formation of PANI-PEO fibers electrospun from a solvent of low volatility. The rods and underlying metal mandrel were both grounded.

Using the new mandrel design, fibers were synthesized successfully for both 9:1 and 4:1 chloroform:

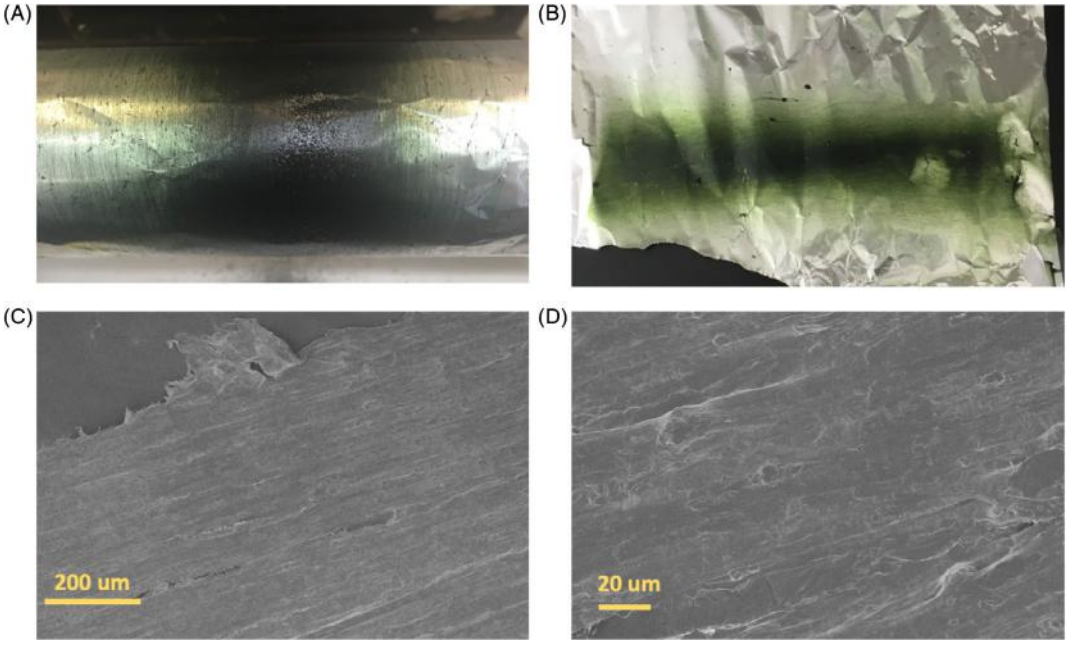

FIGURE 2 Photograph of the polymer sheet formation after electrospinning on a smooth mandrel for 18 h. (A) Electrospinning at 30 kV. (B) Electrospinning at 50 kV. (C) Scanning electron microscopy (SEM) image of sheet formed in electrospinning experiment (A). (D) SEM image of sheet formed in electrospinning experiment (B) [Color figure can be viewed at wileyonlinelibrary.com]

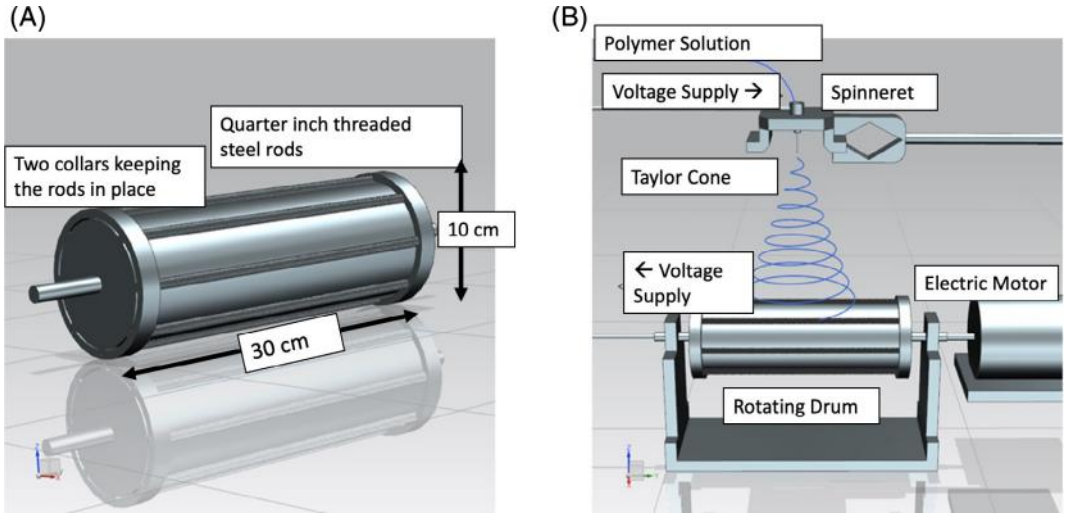

FIGURE 3 An eight-rod design of mandrel and its application in electrospinning. (A) the eight-rod mandrel is shown. (B) the eight-rod mandrel is shown as a rotating drum collector in the electrospinning process [Color figure can be viewed at wileyonlinelibrary.com]

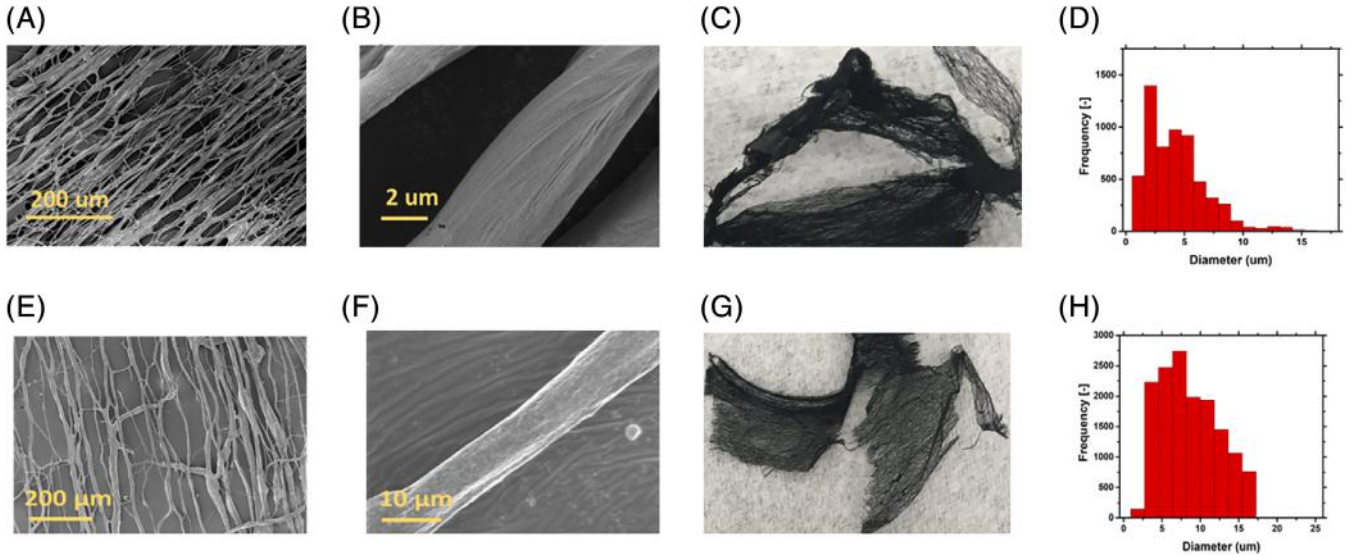

FIGURE 4 Aligned fiber mats prepared by electrospinning on a mandrel with eight rods. For 9:1 polyaniline-poly(ethylene oxide) (PANI-PEO) fibers, (A, B) Scanning electron microscopy (SEM) images (C) photograph (D) diameter distribution. For 4:1 PANI- PEO fibers, (E,F) SEM images (G) photograph (H) diameter distribution [Color figure can be viewed at wileyonlinelibrary.com]

FIGURE 5 Fibers of polyaniline-poly(ethylene oxide) (PANI-PEO) electrospun over different periods of time on an eight-rod mandrel. Alignment of PANI-PEO fibers after (a) 2 h, (B) 6 h, and (C) 12 h (D) 18 h of electrospinning [Color figure can be viewed at wileyonlinelibrary.com]

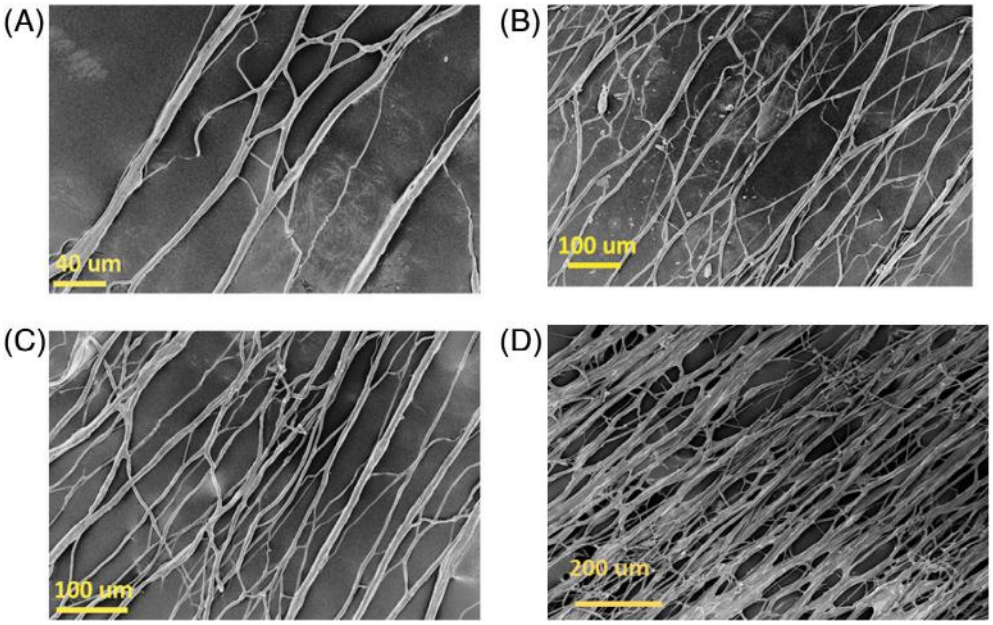

m-cresol samples. The aligned fiber mat could be easily recovered intact from the collector surface (Figure 4(C, G)). The ease of mat recovery was the result of the few attachment points between the mandrel and the fiber mat, as the fiber mat was held above the cylinder surface by the eight axially aligned rods. The recovered mat was completely dry when collected and required no post collection treatment prior to using in a supercapacitor application.[21]

The collected fiber mat exhibited a high level of alignment (Figure 4(A,E)) and retained this alignment even after 18 h of continuous electrospinning. Fiber alignment was perpendicular to the direction of rotation of the mandrel. The individual fibers had a smooth surface (Figure 4 (B,F)) and the fibers showed a fairly tight size distribution with an average fiber diameter of between 5 and 10 µm (Figure 4(D,H)).

The retention of alignment of conductive polymers over long electrospinning times has been especially challenging. No significant change in PANI-PEO fiber alignment was observed between 2 and 18 h of electrospinning as shown in Figure 5(A,D).

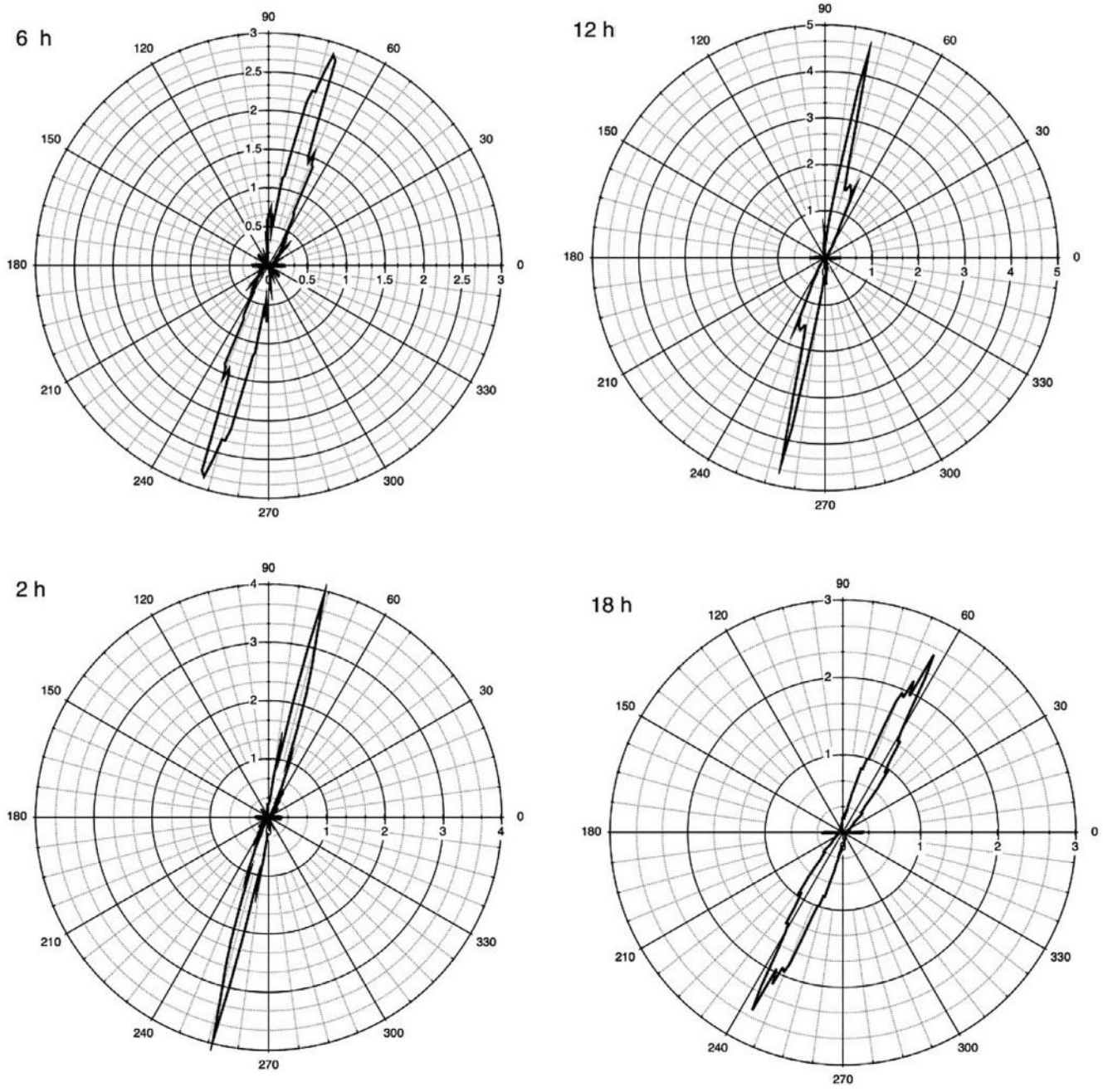

FIGURE 6 Analysis of alignment using MATLAB code source (vector plot)

The alignment of the rods was analyzed using a MATLAB algorithm, Image-Based Fiber Orientation, and Alignment Calculator developed by University of Minnesota[22] (academic use license was obtained). The images were cropped to have square aspect ratios. This insured more accurate plot vectors as described in the algorithm. This program is based on Fourier transform methods (FTM). The magnitude spectrum of the post 2D discrete Fourier transform (DFT)-treated annular section was converted to polar coordinates (r, θ) and then discretized into 1° intervals. Following this, number averaged line intensities were calculated for each interval. These are rotated by 90° to find out the orientation distribution of the spatial domain. From Figure 5, the SEM images show that the fibers are all oriented in the same direction even after 18 h of continuous electrospinning. Figure 6 uses the fiber orientation algorithm to quantify the observations in Figure 5.

The overall fiber orientation angle is a function of how the mat was originally situated in the SEM and so there are some slight differences in the overall orientation in Figure 6(A,D). Of more importance is the spread

in orientation shown in Figure 6 by the thickness or width of the alignment curves. Here, one can see that the width of the curves changes little for deposition times between 2 and 18 h indicating that our assessment of alignment retention in Figure 5 seems correct. The small peaks or spikes in the alignment plots of Figure 6 appear to be an indication of the branching characteristics of the fibers. This kind of branching was seen predominantly in the spinning of PANI using the codopant and may be a consequence of the large disparity in the volatility between the chloroform and m-cresol solvents.

3.2 | Simulation studies

Finite element simulation was next performed to solve the differential equations about the two mandrel geometries and determine the concentration profile of the solvent, the flow field, and the average mass transfer coefficient about the mandrel. Figure 7 shows the evolution of the average mass transfer coefficient once the flow field had been fully established. Within a few seconds, the mass transfer coefficient had reached a steady-state value. Using these steady-state values, the rod-mandrel design showed a mass transfer coefficient about 28-fold higher than the smooth mandrel design. This enhanced mass transfer supports our original theory for why the rod mandrel design works and why it promotes solvent evaporation and fiber independence post deposition.

The concentration profile in Figure 8 show the entire volume between the solid mandrel surface and the rod region is at a high concentration and that the concentration gradient between the mat and the surroundings was higher than could be achieved by deposition on the solid mandrel alone (Figure 8). Streamlines for the flow field surrounding the two geometries are represented by the light-colored lines in the figures.

Simulations were also performed to determine the dependence of the mass transfer coefficient, k_c on the rotation rate of the eight-rod mandrel. The mass transfer coefficient is roughly linearly dependent on the rotation rate (Figure 9) over the limited range used in our experiments and in the simulation. The rotation rate affects the tension applied to the polymer fibers as they are wound about the mandrel. Too high a rotation rate places too much tension on the fiber and snaps it. Thus, the rotation rate can be adjusted only within a rather narrow range

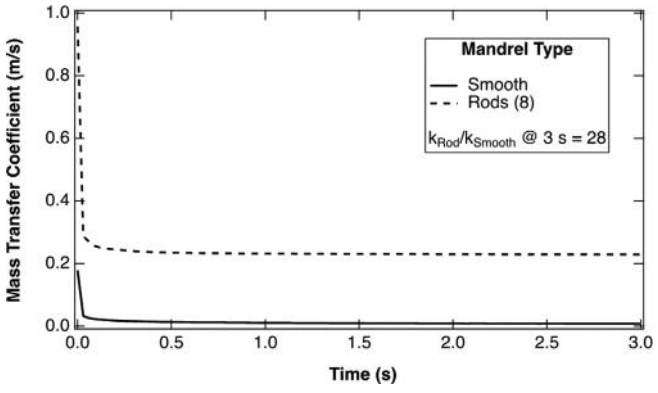

FIGURE 7 Comparison of mass transfer coefficient between a smooth mandrel and a rod-mandrel surface

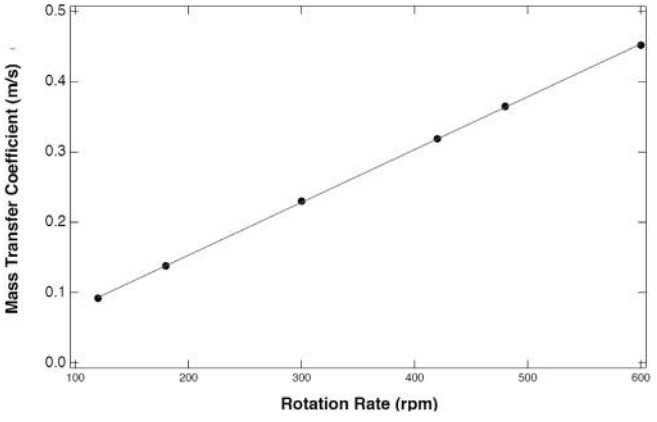

FIGURE 9 Linear dependency of mass transfer coefficient on the rotation rate in rpm of an eight-rod mandrel design

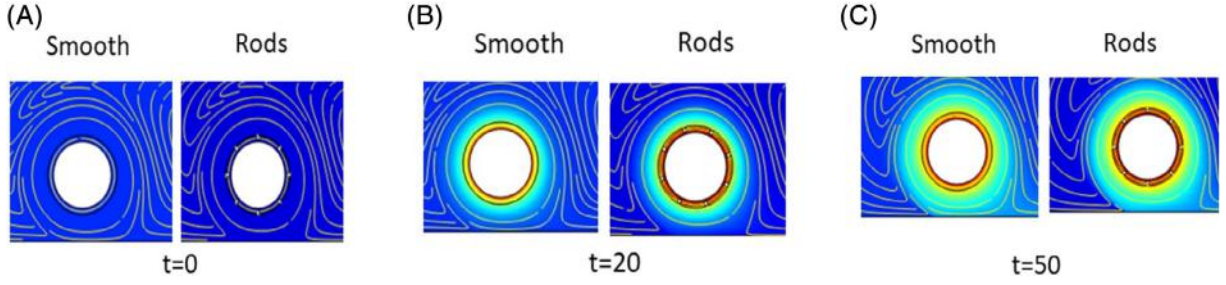

FIGURE 8 The concentration profile of solvent evaporation between the smooth and rod-mandrel surfaces. Color legend: Blue- least concentration, red- maximum concentration. Lines are streamlines for the flow field [Color figure can be viewed at wileyonlinelibrary.com]

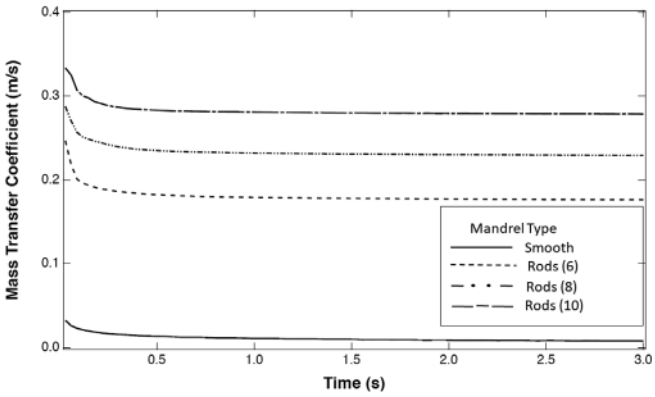

FIGURE 10 Mass transfer coefficient as a function of time for a smooth mandrel and a 6-, 8-, and 10-rod mandrel

depending on the flow rate to the spinneret and in our experiments, there was no feedback loop to automatically adjust the mandrel rotation rate and keep a uniform tension on the fibers.

Simulations also indicate that the mass transfer coefficient increases with the number of rods on the mandrel surface (Figure 10). Mandrel designs with the number of rods ranging from 6 to 10 on the mandrel surface were tested experimentally and simulations indicate that the average mass transfer coefficients ranged from between 0.19 and 0.33 m/s, whereas the smooth mandrel surface had a mass coefficient less than 0.01 m/s.

The number of rods that are most effective depends on more than just an increase in the mass transfer coefficient. When too few rods are used, less than six in our design, the fiber mat will sag onto the solid mandrel surface and fibers will fuse together. When too many rods are used there are too many attachment points making the mat difficult to remove from the mandrel. The rods also act as termination points for the applied electric field. Too many rods provide a field distribution very close to what would be observed for a solid mandrel and, thus, reduce fiber alignment.

4 | CONCLUSIONS

A novel mandrel was designed and used to collect electrospun fibers to form thick and tack-free, aligned mats from relatively high boiling point, low volatility solvents. This eight-rod mandrel design was successful in electrospinning polymer fiber mats from a mixture of chloroform and *m*-cresol. These fiber mats could be easily recovered from the mandrel since they are suspended between the rods even after 18 h of electrospinning. The fiber mats obtained are advantageous for a variety of applications such as supercapacitor electrodes and gas sensing electrodes, where these fiber mats can be used as free-standing electrodes. An analysis of the flow and concentration fields surrounding the mandrel designs indicates that the increased mass transfer coefficient associated with the threaded-rod mandrel design is responsible for its improved performance.

ACKNOWLEDGMENTS

This research was funded by grants from NASA 80NSSC18K0332 and by Rensselaer Polytechnic Institute. The authors acknowledge the following people for their assistance in handling characterization instruments: Mr. David Frey from the center for integrated electronics SEM assistance and William Flaherty for his help in building the electrospinning mandrel.

CONFLICT OF INTEREST

The authors declare no potential conflict of interest.

ORCID

Somdatta Bhattacharya https://orcid.org/0000-0002-4505-9407

REFERENCES

[1] D. Li, Y. Xia, *Adv. Mater.* **2004**, *16*, 1151.
[2] P. Kampalanonwat, P. Supaphol, *ACS Appl. Mater. Interfaces* **2010**, *2*, 3619.
[3] S. Chaudhari, Y. Sharma, P. S. Archana, R. Jose, S. Ramakrishna, S. Mhaisalkar, M. Srinivasan, *J. Appl. Polym. Sci.* **2013**, *129*, 1660.
[4] Z. Tong, L. Huang, W. Lei, H. Zhang, S. Zhang, *J. Energy Chem.* **2021**, *54*, 254.
[5] E. Sharifisamani, F. Mousazadegan, R. Bagherzadeh, M. Latifi, *Polym. Eng. Sci.* **2020**, *60*, 1520.
[6] N. Babincová, O. Jirsák, M. Babincová, P. Babinec, M. Šimaljaková, *J. Physiol. Sci.* **2020**, *75*, 587.
[7] H. Ma, B. S. Hsiao, B. Chu, *J. Membr. Sci.* **2014**, *452*, 446.
[8] X. Xie, Y. Chen, X. Wang, X. Xu, Y. Shen, A. U. R. Khan, A. Aldalbahi, A. E. Fetz, G. L. Bowlin, M. el-Newehy, X. Mo, *J. Mater. Sci. Technol.* **2020**, *59*, 243.
[9] R. Bilginer, A. A. Yildiz, *Mater. Lett.* **2020**, *276*, 128191.
[10] T. Subbiah, G. S. Bhat, R. W. Tock, S. Parameswaran, S. S. Ramkumar, *J. Appl. Polym. Sci.* **2005**, *96*, 557.
[11] Y. Zhang, Z. M. Huang, X. Xu, C. T. Lim, S. Ramakrishna, *Chem. Mater.* **2004**, *16*, 3406.
[12] P. Katta, M. Alessandro, R. D. Ramsier, G. G. Chase, *Nano Lett.* **2004**, *4*, 2215.
[13] A. E. Farah, B. S. Lalia, R. Hashaikeh, *Desalination* **2015**, *356*, 15.
[14] S. L. Shenoy, W. D. Bates, H. L. Frisch, G. E. Wnek, *Polymer* **2005**, *46*, 3372.
[15] S. H. Lee, J. W. Yoon, M. H. Suh, *Macromol. Res.* **2002**, *10*, 82.
[16] S. I. Abd Razak, I. F. Wahab, F. Fadil, F. N. Dahli, A. Z. Md Khudzari, H. Adeli, *Adv. Mat. Sci. Eng.* **2015**, *2015*, 356286.
[17] Y. Zhou, H. Wang, J. He, K. Qj, B. Ding, **2019**, *239*, 1.
[18] P. Andersson, M. Berggren, T. Kugler, *Appl. Phys. Lett.* **2003**, *83*, 1307.

[19] H. Di Zhang, C. C. Tang, Y. Z. Long, J. C. Zhang, R. Huang, J. J. Li, Z. Gu, *Sens. Actuators, A Phys.* **2014**, *219*, 123.
[20] D. Li, Y. Wang, Y. Xia, *Nano Lett.* **2003**, *3*, 1167.
[21] S. Bhattacharya, I. Roy, A. Tice, C. Chapman, R. Udangawa, V. Chakrapani, J. L. Plawsky, R. J. Linhardt, *ACS Appl. Mater. Interfaces* **2020**, *12*, 19369.
[22] E. A. Sander, V. H. Barocas, *J. Biomed. Mater. Res. Part A* **2009**, *88*, 322.

How to cite this article: Bhattacharya S, Woodcock C, Linhardt RJ, Plawsky JL. Enhanced mandrel design for electrospinning aligned fiber mats from low volatility solvents. *Polym Eng Sci*. 2021;61:793–801. https://doi.org/10.1002/pen.25622